Available online at www.sciencedirect.com
SCIENCE DIRECT
Trans. Nonferrous Met. Soc. China 18(2008) 665−673
Transactions of Nonferrous Metals Society of China
www.csu.edu.cn/ysxb/

Elasto-plastic finite element analysis of squaring circular tube

HUANG Yuung-ming(黄永明)

Department of Mechanical and Computer-Aided Engineering, St. John's University, Taipei 25135, China

Received 27 August 2007; accepted 3 December 2007

Abstract: The flow rule of Prandtl-Reuss was adopted and incremental elasto-plastic finite-element analysis formulation of Coulomb's friction law combining the finite deformation theory was established, and Lagrangian formulation for simulating the squaring process of circular tube was updated. Incremental Coulomb's friction law was used in the global stiffness matrix to solve the sliding-sticking state of friction at the boundary contact interface. During the squaring process, the linear factor r_{min} was adopted to solve the non-linear boundary problems of changing node contact and separation, elasto-plastic transient situation in an element and the non-linear constitutive behavior of material so as to make each reasonable increment of the punch meet the demand of calculation for linear increment. The squaring process of circular tube, load distribution and final shape of work piece after unloading were simulated by this mode and compared with research data. It is known that the circular tube with higher geometrical ratio (R/t) could be pressed into symmetric square tube without collapse. This result can provide reference for the analysis of this process and evaluation and improvement of product defects.

Key words: elasto-plasticity; finite-element; square tube; collapse

1 Introduction

With the convenience of connecting and picking, efficiency of contacting heat conduction, strength of geometric twist and high-energy vibration damping, square tubes are widely used as exhaust component of motorcycles and automobiles, support beam, suspension system, desk and chair or bookshelf. The square tube made by piercing or extrusion would produce the non-uniform property in the transverse direction due to the shear deformation occurring in shaping. In this study, circular tubes were utilized and pressing method was adopted to square the seamless circular tube directly (Fig.1) so as to reduce cost, add utilization methods and prevent vertical shear difference of tube.

There are several methods of exerting pressure according to the location of tube such as shaping at tube end[1−4] or pressing circular tube[5−8] with two rigid, parallel plates on the side of tube for discussing the occurrence of the character of circular tube collapse, energy absorbing method[9−12] for discussing application of circular tube and LEU[13] who discussing influence of the parameter on squaring circular tube simply with finite element method. The primary task of the preliminary discussion on the squaring process of circular tube was to analyze the deformation history of squared transverse of circular tube and load distribution. The non-linear problem comprised: 1) geometrical non-linear behavior due to large displacement, large rotation and large strain; 2) the non-linear constitutive behavior of material with elasto-plastic deformation; 3) friction and changing situation of contact-separation due to contact interface. Due to large capacity of memory and processing speed of PC, finite element is suitable for solving such non-linear problems.

This study conducted radially compressed press-forming to circular tube between two V-shape dies to make a square tube without collapse and fit-contacting the mold during the whole pressing process (Fig.1(c)). Collapse of tube surface may be due to geometric effect, property of the material and contact friction on symmetrical sections of the square tube. Since not much work had been carried out on squaring circular tube, the main aim of this study was to establish incremental elasto-plastic finite-element analysis formulation of Coulomb's friction law and adopted r_{min} method of YAMADA et al[14] to global stiffness matrix to solve the

Foundation item: Project(95-2221-E-129-001) supported by the National Science Council, Taiwan, China
Corresponding author: HUANG Yuung-ming; Tel: +886-28013131-6724; E-mail: hyming@mail.sju.edu.tw

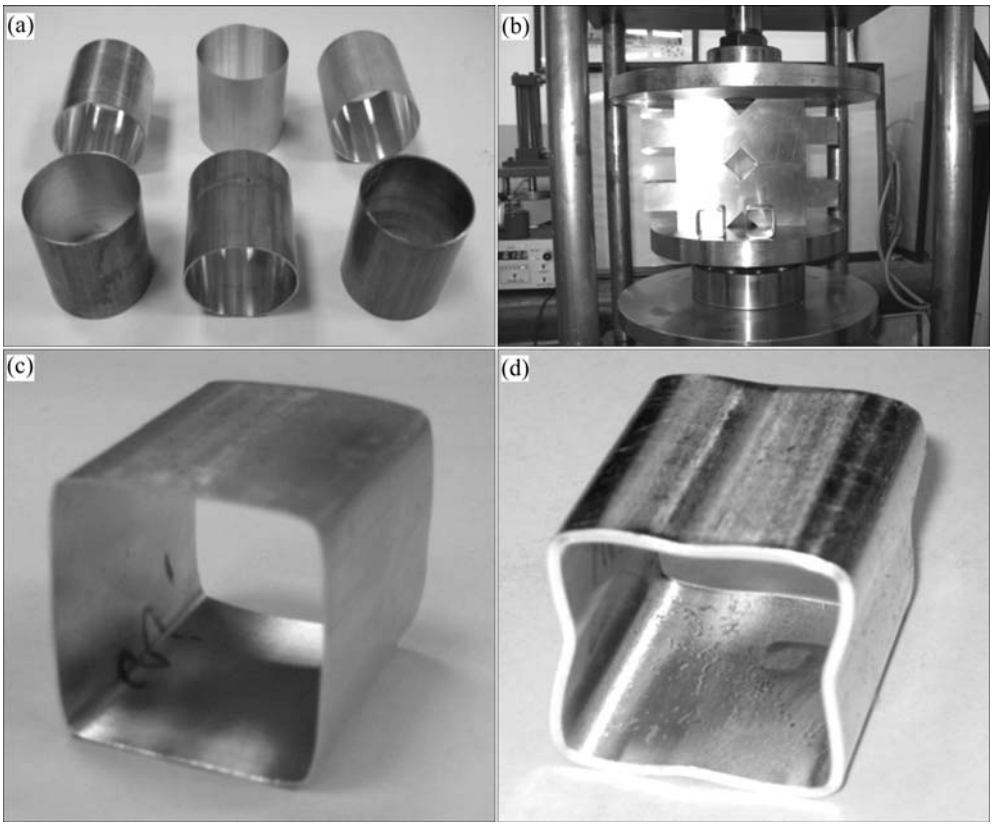

Fig.1 Circular copper tube and aluminum tube (a), experimental equipment (b), aluminum without collapse (c) and aluminum with collapse (d)

problems of contact friction, contact-separation of tube and die, limits of material element rotating increment allowance or strain increment allowance and elasto-plastic transient situation in order to meet the demand of calculation for linear increment and acquire correct and complete boundary contact situation. Such method could be used in simulating the deformation history of squaring process of circular tube, load distribution and discussion on the influence of process parameters.

2 Basic theory

The J_2-flow constitutive equation is

$$\tilde{\tau}_{ij}=\frac{E}{1+\upsilon}\cdot\left[\delta_{ik}\delta_{jl}+\frac{\upsilon}{1-2\upsilon}\delta_{ij}\delta_{kl}-\frac{3\alpha\left(\frac{E}{1+\upsilon}\right)\sigma'_{ij}\sigma'_{kl}}{2\bar{\sigma}^2\left(\frac{2}{3}H'+\frac{E}{1+\upsilon}\right)}\right]\dot{\varepsilon}_{kl} \quad (1)$$

The J_2-flow law is simple and all material constants were determined by the uniaxial tension test only. The relationship between equivalent stress $\bar{\sigma}$ and equivalent plastic strain $\bar{\varepsilon}_{\mathrm{p}}$ of the material is represented by an n-power law of the form in order to model the hardening behavior:

$$\bar{\sigma}=K\bar{\varepsilon}_{\mathrm{p}}^{n} \quad (2)$$

where n denotes the strain hardening exponent and K is a material constant.

The virtual work rate equation, with respect to a deformed configuration of the updated Lagrangian equation at the Jaumann rate of Cauchy stress and the body forces being neglected, can be expressed as[15]

$$\int_V(\tilde{\tau}_{ij}-2\sigma_{ik}\dot{\varepsilon}_{kj})\delta\dot{\varepsilon}_{ij}\mathrm{d}V+\int_V\sigma_{jk}L_{ik}\delta L_{ij}\mathrm{d}V=\int_{S_{\mathrm{f}}}\dot{\bar{t}}_i\delta v_i\mathrm{d}S \quad (3)$$

The general governing finite element equation for the metal forming process can be derived from the virtual work rate equation of the updated Lagrangian equation (Eqn.(3)). By coupling the elasto-plastic constitutive equation for anisotropic material adopted from $\tilde{\sigma}_{ij}=D^{\mathrm{ep}}_{ijmn}\dot{\varepsilon}_{mn}$ [16], Eqn.(1) can be written in matrix form as

$$\int_V\{\delta\dot{\varepsilon}\}([\boldsymbol{D}^{\mathrm{ep}}]-[\boldsymbol{Q}]\{\dot{\varepsilon}\})\mathrm{d}V+\int_V\{\delta L\}^{\mathrm{T}}[\boldsymbol{G}]\{L\}\mathrm{d}V=\int_{S_{\mathrm{f}}}\{\delta v\}^{\mathrm{T}}\{\dot{\bar{t}}\}\mathrm{d}S \quad (4)$$

where $[\boldsymbol{Q}]$ and $[\boldsymbol{G}]$ are defined as stress-correction

matrices due to the current stress at all stages of deformation, $[\boldsymbol{D}^{\mathrm{ep}}]$ is the matrix form of the coefficient tensor and represents the tangent modulus of the rate of elasto-plastic tensor for the anisotropic material.

The aforementioned problem is solved in the standard way: Eqn.(4) is integrated from time t to $t+\Delta t$, where Δt is a small time increment. All rate quantities are simply replaced by incremental quantities, assuming that rates are maintained constant in each incremental step. Standard finite element discretization, and the introduction of an elemental shape function enable Eqn.(4) to be replaced by a system of a algebraic equations:

$$[\boldsymbol{K}]\{\Delta u\}=\{\Delta F\} \tag{5}$$

where

$$[\boldsymbol{K}]=\sum_{e}\int_{V^e}[\boldsymbol{B}]^{\mathrm{T}}([\boldsymbol{D}^{\mathrm{ep}}]-[\boldsymbol{Q}])[\boldsymbol{B}]\mathrm{d}V+\sum_{e}\int_{V^e}([\boldsymbol{E}]^{\mathrm{T}}-[\boldsymbol{G}])[\boldsymbol{E}]\mathrm{d}V \tag{6}$$

$$\{\Delta F\}=(\sum_{<e>}\int_{S^{<e>}}[\boldsymbol{N}]^{\mathrm{T}}\{\dot{\bar{t}}\}\mathrm{d}S)\Delta t \tag{7}$$

The friction condition between the workpiece and tool plays an important role in the squaring process. In order to take the friction effect into account, a modified Coulomb friction law proposed by ODEN and PRIES[17] is adopted. Two contact friction states such as sticking and sliding can be treated well by making use of this analytical friction law in an incremental way. Global coordinates (x, y) and local coordinates (l, n) are used to describe the nodal force, displacement and element stress, strain, etc. The l-axis is consistent with the longitudinal direction of the sheet; the n-axis is perpendicular to the l-axis. The nodal force acting towards the contact node of the sheet is considered to slide along the curve tool surface, which can be resolved into normal and tangential components f_n and f_l:

$$\boldsymbol{F}=f_l\,\boldsymbol{l}+f_n\,\boldsymbol{n} \tag{8}$$

where $\boldsymbol{n}$ is the outward vector normal to the tool surface. The tangential force, with its direction coinciding with the sliding direction, was obtained by the modified Coulomb's friction law to treat the alteration of sliding-sticking state of friction:

$$f_l=\pm\mu\, f_n\,\phi\left(\Delta u_l^{\mathrm{rel}}\right) \tag{9}$$

The function $\phi(\Delta u_l^{\mathrm{rel}})$ is defined as

$$\phi\left(\Delta u_l^{\mathrm{rel}}\right)=\tanh\left(\frac{\Delta u_l^{\mathrm{rel}}}{(VCRI/3)}\right) \tag{10}$$

The function $\tanh\left(\Delta u_l^{\mathrm{rel}}/(VCRI/3)\right)$ denotes an analytical hyperbolic function, which is used to treat the discontinuity of sliding and sticking, and $VCRI$ is the limit displacement increment for quasi-sticking. $\Delta u_l^{\mathrm{rel}}$ is the sliding displacement increment related to the tool movement:

$$\Delta u_l^{\mathrm{rel}}=\Delta u_l-U\sin\theta \tag{11}$$

where θ is the angle between the l-axis and the horizontal axis; Δu_l is the tangential displacement increment of the contact node and U is the tool displacement increment.

$$\Delta\boldsymbol{F}=\Delta f_n\boldsymbol{n}+f_n\Delta\boldsymbol{n}+\Delta f_l\boldsymbol{l}+f_l\Delta\boldsymbol{l} \tag{12}$$

where

$$\Delta\boldsymbol{n}=\pm\frac{\Delta u_l^{\mathrm{rel}}}{\rho}\boldsymbol{l},\ \Delta\boldsymbol{l}=\pm\frac{\Delta u_l^{\mathrm{rel}}}{\rho}\boldsymbol{n} \tag{13}$$

$$\Delta f_l=\pm\left[\Delta f_n\tanh\left(\frac{\Delta u_l^{\mathrm{rel}}}{VCRI/3}\right)+\frac{f_n\Delta(\Delta u_l^{\mathrm{rel}})}{(VCRI/3)\cosh^2\dfrac{\Delta u_l^{\mathrm{rel}}}{VCRI/3}}\right] \tag{14}$$

where ρ denotes the radius of the tool and "$\pm$" depends on the curvature of tool.

The above equations obviously include a correction term, which should be incorporated into the relative component of the global stiffness matrix with respect to the contact node by

$$\begin{bmatrix} k & \cdots & \cdots \\ \cdots & k_{11}\pm\dfrac{f_n^{(i-1)}}{\rho} & k_{12} \\ \cdots & k_{21}\mp\dfrac{f_l^{(i-1)}}{\rho} & k_{22} \end{bmatrix}\begin{Bmatrix} \cdots \\ \Delta u_l \\ \Delta\bar{u}_n \end{Bmatrix}=\begin{Bmatrix} \cdots \\ \pm\dfrac{f_n^{(i-1)}U\sin\theta}{\rho}+\Delta f_l^{(i-1)} \\ \mp\dfrac{f_l^{(i-1)}\ U\sin\theta}{\rho}+\Delta f_n^{(i)} \end{Bmatrix} \tag{15}$$

where $\Delta\bar{u}_n$ is a prescribed displacement increment of the contact node in the normal direction of the contact boundary, and equals $U\cos\theta$; i denotes the current incremental step and $i-1$ denotes the previous incremental step. In the solution scheme, the friction force increments of the contact node are evaluated iteratively, i.e., Δf_l is given at each iteration by the value

obtained in the former iteration step.

That the stiffness matrix in Eqn.(15) is asymmetric requires special consideration. In the solution scheme of the present paper, the components of the increment of contact nodal friction forces are prescribed iteratively by Eqn.(14).

3 Numerical analysis

The experimental setup and the analytical model of the squaring circular tube are based on the plane strain condition as shown in Fig.2. Fig.2(a) shows the profile of the punch head and the initial shape for simulation. Fig.2(b) shows the various boundary conditions of deformed tube at a certain stage of squaring. Because of the symmetry of tube, only a quarter portion of tools and tube are molded. Table 1 lists the material conditions of this simulation.

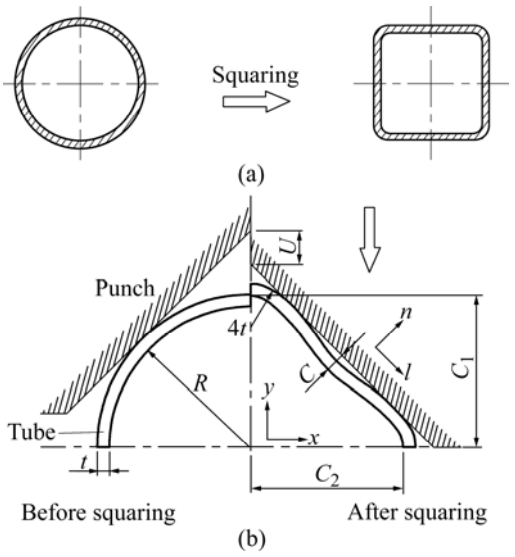

Fig.2 Schematic diagram of squaring tube showing initial (a) and deformed conditions (b)

Table 1 Material properties of tube

Material	Yield stress/ MPa	Poisson ratio, υ	Elastic modulus, E/GPa	Stress—plastic strain relation
Aluminum	165.3	0.34	75	$\bar{\sigma} = 673.5\bar{\varepsilon}_p^{0.927}$
Hard copper	445.0	0.34	112	$\bar{\sigma} = 3628.6\bar{\varepsilon}_p^{0.987}$

The contact condition must remain unchanged within one incremental step. In order to satisfy this requirement, the r_{min} technique proposed by YAMADA et al[7] is adopted and extended to handle the elasto-plastic and contact problems. The increment of each loading step is controlled by the smallest value of the following six values:

$$r_{min}=\min\{r_1, r_2, r_3, r_4, r_5, r_6\} \quad (16)$$

where r_1 constrains the state of element stress to be just on the yielding surface when the element stress is greater than the yielding stress; r_2 and r_3 constrain the largest principle strain and the rotation increment, respectively. To the linear relation, r_4 causes the free nodes to contact with the tools; r_5 causes the contact node to depart from the tool surface and r_6 provides alternation to the friction state from sliding to sticking for the contacted node along the tool/tube interface.

In order to know the final shape or the springback behavior, the unloading process is executed by assuming that all elements are reset to be elastic. The force of the contact node is reversed to become the prescribed force boundary condition. All tools are removed for the elastic unloading procedure.

4 Results and discussion

A comparison of punch load of the experiments, using zinc stearate lubricant, with that in the FEM simulation by assuming the friction coefficient to be 0.05 is shown in Fig.3. It can be seen that the load of small R/t is larger than that of large R/t. If R/t has the same value, load of copper tube will be larger than that of aluminum tube, which shows influence of the material. Good agreement between the experimental and calculated results is obtained in this relationship.

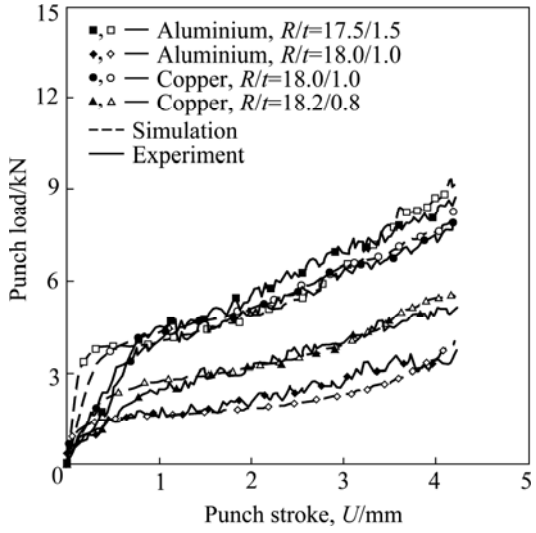

Fig.3 Relationship of punch load to punch stroke in squaring process under various materials and R/t conditions

When compression proceeds in the squaring process, the contact points of load application move out around the tube, and it would have the effect of shortening the arm, which has produced high moments. In the meantime, the geometric constraints as a small edge radius produce in vertical and horizontal directions of diameter of tube,

which will increase its degree with compression. If the material strain hardens in the plastic, the effect will still increase the load carrying capacity under severe compression. Generally, the tube may be flattened in the contact zone of V-shape punch without separation and a square tube would be successfully shaped. But in some process conditions, separation would occur upon increasing the separation.

Squaring process of the two materials of circular tubes and the final shape of the square tube after the springback were simulated according to the material properties listed in Table 1 and the FE code to examine whether collapse would appear (Fig.4). Nodal displacement increment of tube is shown in Fig.5. All simulations of punch stroke were based on the condition of hypothesis that deformed edge of square tube was a quarter circle. During the process of squaring compression, the outer radius of edge being four times

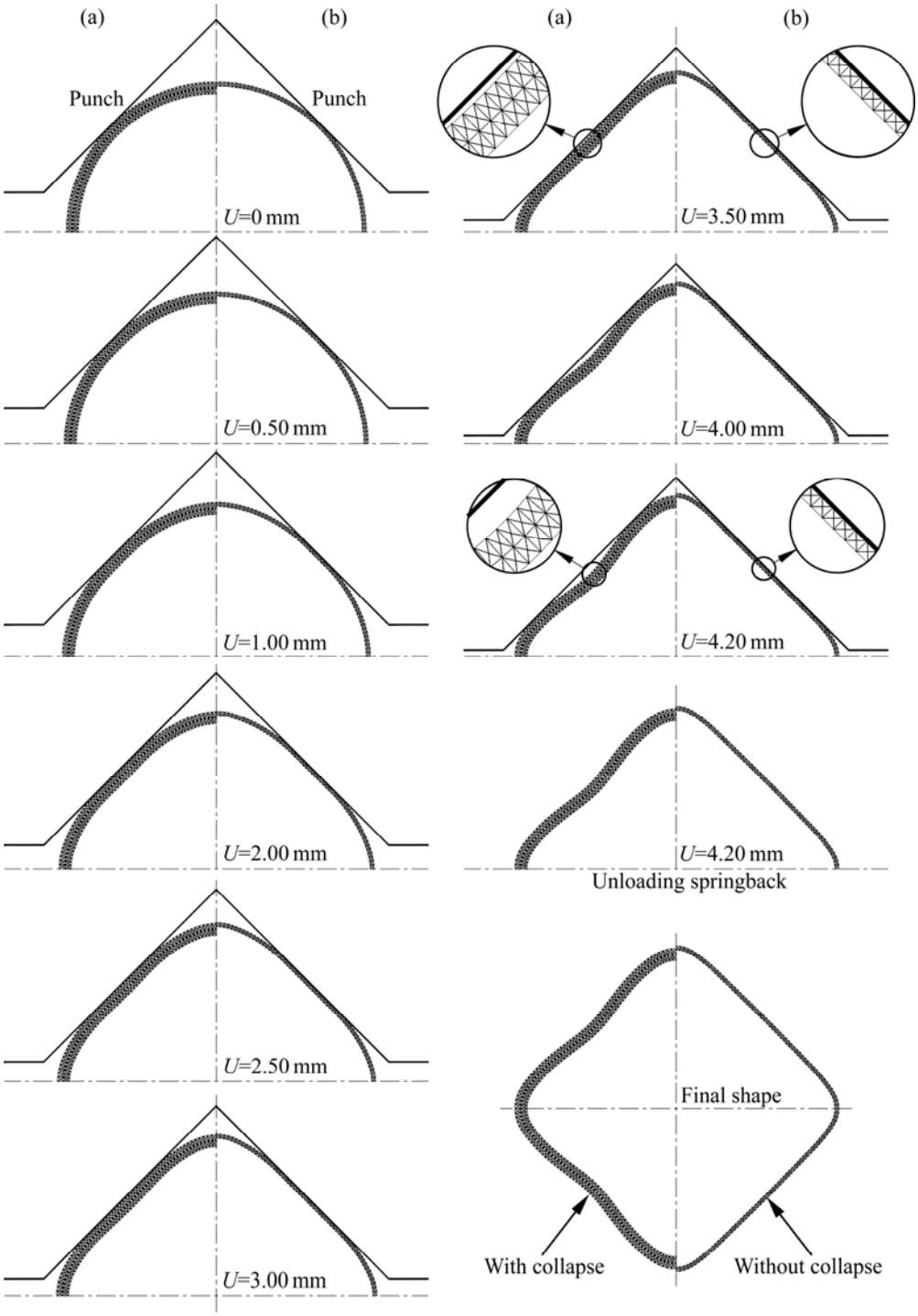

Fig.4 Deformed increment in geometries of squaring processes under condition of μ=0.05 (Both cases show springback after unloading in final stage U=4.20 mm): (a) Aluminum with collapse (R/t=11.67); (b) Aluminum without collapse (R/t=37.0)

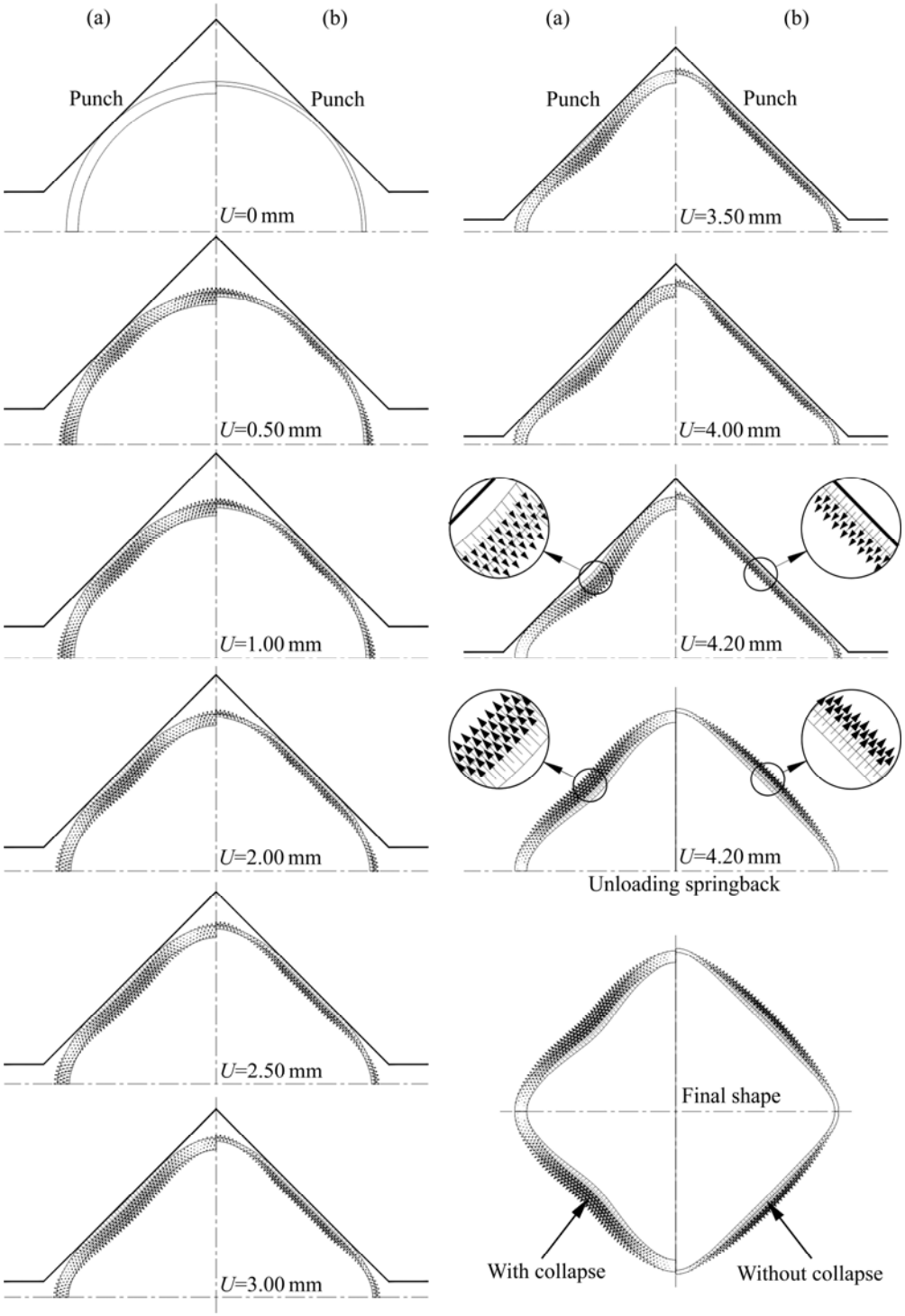

Fig.5 Nodal velocity distribution increment with μ=0.05 (Both cases show springback after unloading in final stage U=4.20 mm): (a) Aluminum with collapse (R/t=11.67); (b) Aluminum without collapse (R/t=37.0)

tube thickness was used to decide punch stroke in order to approximately simulate critical situation of squaring deformation and prevent pure bending. Figs.4 and 5 showed that the punch stoke U within the range of 0.5 mm to 4.2 mm collapsed and deformed when geometrical ratios (R/t) were different. Fig.4(a) indicated that the squaring process with R/t=11.67 showed obvious collapse and deformation within 3.50−4.20 mm. Separation appears in the middle between tube and punch and the degree increased upon continued compression. Since the arc of the edge was easy to be strengthened during the squaring process and turned into the beam loaded with transverse pressure with fixed ends, moment and bend would appear and result in collapse. When R/t was 37.0, from start of compression to the final step of squaring process, tube of contact area

and V-shape punch fitted perfectly without any collapse (Fig.4(b)). This proved that the difference of R/t would influence forming of tube. Figs.1(c) and 1(d) could also be used to prove the situation of collapse. In Figs.5(a) and 5(b), when U was 4.20 mm, the respective directions of the two nodes before and after unloading were opposite (springback).

Upon continuing the squaring process, deformation with different degrees would appear at transverse and vertical edges, because contact friction and geometrical limit would result in asymmetry section on the square tube. The C_1/C_2 of asymmetry square tube was called deviation ratio, which was adopted in measuring the asymmetry degree of compressing tube.

Deviation ratio with different process parameters is shown in Fig.6, which revealed that small R/t and large friction coefficient (μ=0.35) resulted in large degree of asymmetry. Within 1−2 mm, the punch stroke showed the maximum asymmetry, i.e. the C_1/C_2 ratio was the minimum of 0.83. Fig.7 shows deformation and nodal speed distribution. According to Fig.6, larger friction coefficient resulted in larger deviation during the process but the ratio would be symmetrical ($C_1/C_2 \approx 1$) and within the allowance of 5% at the end of the process. However, it still showed influence of friction on symmetry of squaring process.

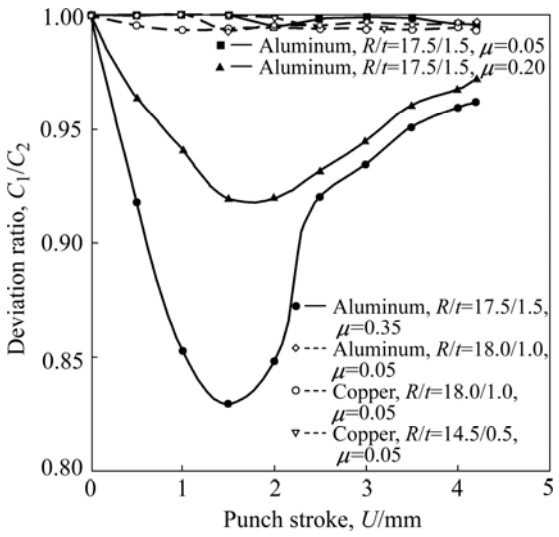

Fig.6 Distribution of deviation ratio C_1/C_2 along punch stroke U under various material parameters

The C/t means collapse ratio, in which C is the maximum separating distance between tube and punch and t is the thickness of the tube (Fig.2). The collapse ratio is used to measure the degree of collapse under the situation of collapse during the squaring process. Large collapse ratio means larger degree of collapse. Fig.8 reveals the change in collapse during the squaring process with different parameters. Except for copper tube and the situations of R/t=14.5/0.5 and μ=0.05, collapse

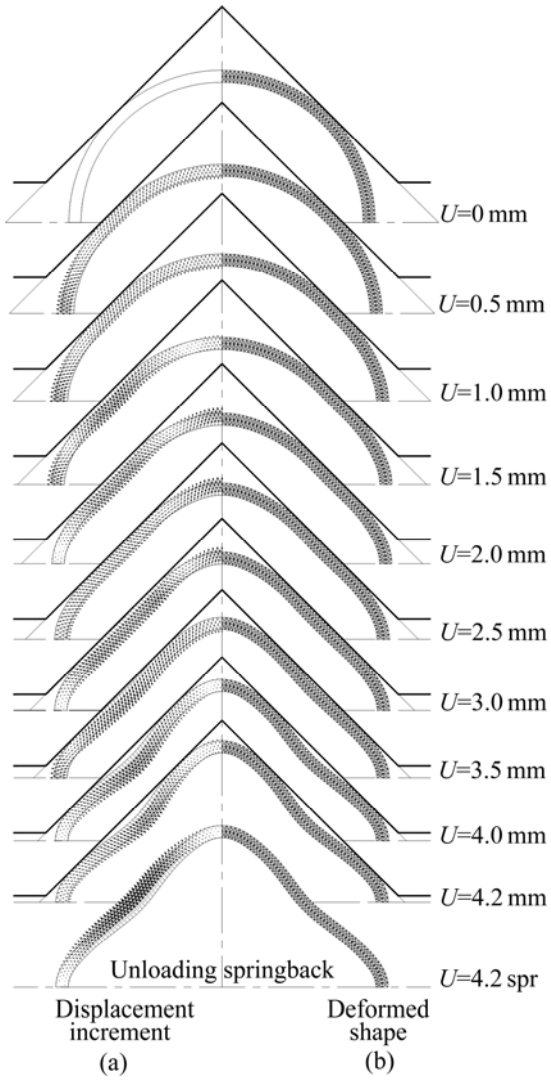

Fig.7 Case of squaring process with asymmetric shape which corresponds to curve marked by symbol "●" in Fig.6

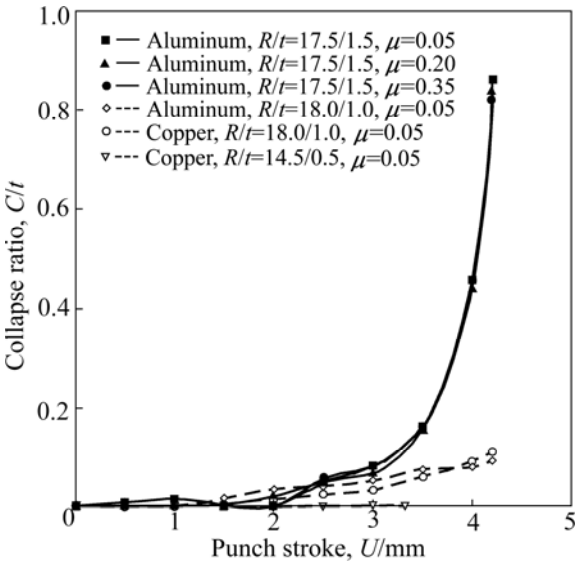

Fig.8 Distribution of collapse ratio C/t along punch stroke U with various materials under different R/t and μ

would appear in other materials. Aluminum material with R/t=17.5/1.5 (μ=0.05, μ=0.20 and μ=0.35), showed the same degree of collapse. This proved that the geometrical ratio of circular tube played an important role in collapse effect.

Fig.9 showed that under R/t=6.33 and with large friction coefficient, larger degree of asymmetry would appear. Within the range from R/t=6.33 to R/t=22.75, the degree of asymmetry would increase progressively upon increasing the friction coefficient. When the R/t was larger than 22.75, the friction coefficient would only slightly influence the degree of asymmetry. In spite of such situation, the degree of asymmetry could remain within the allowance of 5%. Fig.10 shows the influence of geometrical ratio on collapse ratio. Within the range from R/t=10.0 to R/t=14.0, the collapse ratio was large with different values of μ. When R/t was larger than 22.75, the collapse ratio became small. This proved that R/t larger than 22.75 resulted in a perfect square tube without collapse.

Figs.11 and 12 show the influence of friction coefficient μ on the deviation ratio C_1/C_2 and collapse ratio C/t. Fig.11 showed that the deviation ratio C_1/C_2 decreased upon increasing the friction coefficient μ, which meant the increase of asymmetry. Small R/t showed more obvious situation of asymmetry. When R/t was large, deviation ratio was within 5%, which showed little influence. Fig.12 showed that large R/t did not show any collapse, small R/t brought slight collapse, and R/t=11.67 showed obvious collapse.

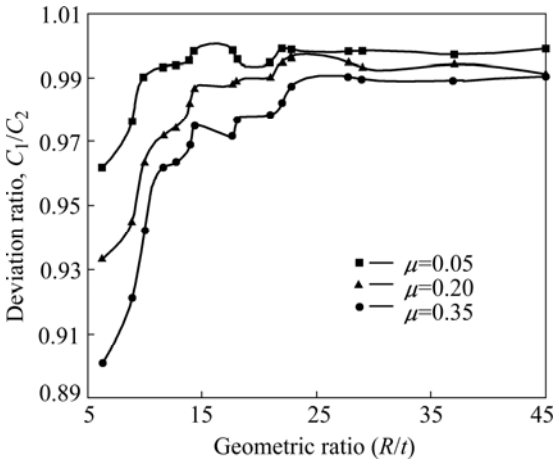

Fig.9 Effect of geometric ratio R/t on deviation ratio C_1/C_2 with various μ

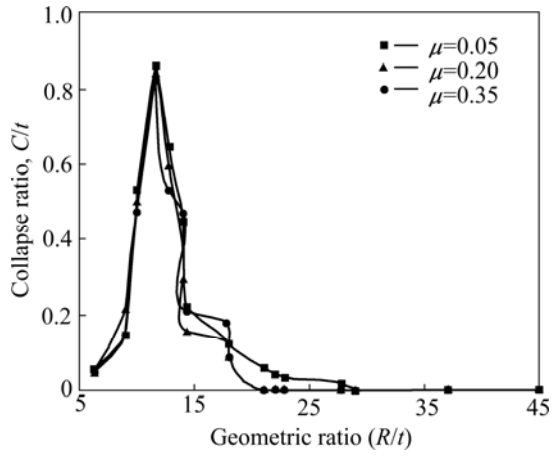

Fig.10 Effect of geometric ratio R/t on collapse ratio C/t with various μ

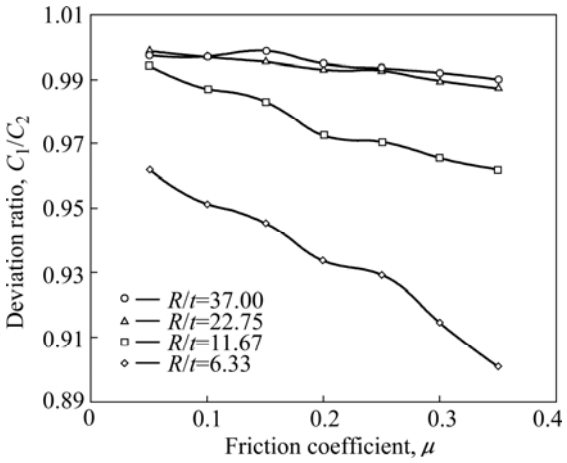

Fig.11 Effect of friction coefficient μ on deviation ratio C_1/C_2 with various R/t

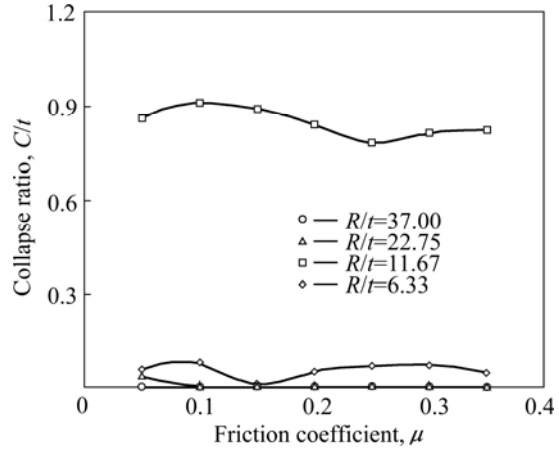

Fig.12 Effect of friction coefficient μ on collapse ratio C/t with various R/t

According to Fig.8 and Fig.12, large R/t could acquire square tube without collapse. According to Fig.9 and Fig.11, large R/t and small μ could ensure asymmetry degree of asymmetrical square tube within the allowance of 5%. In other words, although the influence and interaction between R/t and μ was complicated, it was positive that circular tube with large R/t could be easily pressed into symmetrical square tube without collapse.

5 Conclusions

1) An extended r_{min} technique can trace adequately the entire deformation history of the squaring process.

2) The simulated result of the relationship between punch load and punch travel agrees well with the experimental results.

3) Geometrical ratio R/t plays an important role in collapse; however, it is not influenced by the friction coefficient. Perfect square tube without collapse calls for R/t larger that 22.75.

4) When the geometrical ratio is small (e.g. $R/t \leqslant 11.67$), increasing the friction coefficient will increase the asymmetry degree. When the geometrical ratio is large (e.g. $R/t \geqslant 11.67$), the influence of friction coefficient on the asymmetry degree is slight and the asymmetry degree can be kept within 5%.

Nomenclature

$\widetilde{\tau}_{ij}$	Jaumann rate of Cauchy stress;
σ_{ij}	Cauchy stress;
σ'_{ij}	Deviatoric part of σ_{ij};
H'	Strain-hardening rate;
L_{ij}	Velocity gradient ($=\partial v_j/\partial x_i$);
E	Elastic modulus;
υ	Poisson ratio;
α	Value of unity for plastic state and zero for elastic state or unloading;
v_i	Velocity;
x_i	Spatially fixed Cartesian coordinate;
$\dot{\bar{t}}_i$	Rate of nominal traction;
V	Material volume;
$\dot{\varepsilon}_{ij}$	Strain rate;
$[\boldsymbol{N}]$	Shape function matrix;
$\{\Delta u\}$	Nodal displacement increment;
$[\boldsymbol{B}]$	Strain rate-velocity matrix;
$[\boldsymbol{E}]$	Velocity gradient-velocity matrix;
r_{p}	Punch radius;
r_{d}	Die radius;
S_{f}	Surface on which traction prescribed;
$[\boldsymbol{K}]$	Global tangent stiffness matrix;
$[\boldsymbol{D}^{\mathrm{ep}}]$	Elemental elasto-plastic constitutive matrix
$\{\Delta F\}$	Increment of nominal force;
$[\boldsymbol{Q}]$ and $[\boldsymbol{G}]$	Stress correction matrices.

References

[1] MISCOW F P C, AL-QURESHI H A. Mechanics of static and dynamic inversion process [J]. Int J Mech Sci, 1997, 39(2): 147−161.

[2] LEU D K. The curling characteristics of static inside-out inversion of metal tubes [J]. Int J Mach Tools & Manu, 2000, 40: 65−80.

[3] HUANG Y M. Finite element analysis of tube inward curling process by conical dies [J]. J Mater Pro Tech, 2005, 170: 616−623.

[4] YU H P, LI C F. Finite element analysis of free expansion of aluminum alloy tube under magnetic pressure [J]. Trans Nonferrous Met Soc China, 2005, 15(5): 1040−1044.

[5] REID S R., DREW S L K, CARNEY J F III. Energy absorbing capacities of braced metal tubes [J]. Int J Mech Sci, 1983, 25(9/10): 649−667.

[6] WATSON A R, REID S R, JOHNSON W, THOMAS S G. Large deformations of thin-walled circular tubes under transverse loading (II) [J]. Int J Mechl Sci, 1976, 18: 387−397.

[7] WATSON A R, REID S R, JOHNSON W, THOMAS S G. Large deformations of thin-walled circular tubes under transverse loading (III) [J]. Int J Mech Sci, 1976, 18: 501−509.

[8] JOHNSON W, REID S R, REDDY T Y. The compression of crossed layers of thin tubes [J]. Int J Mech Sci, 1977, 19: 423−437.

[9] MUTCHLER L D. Energy absorption of aluminium tubing [J]. Trans ASME J App Mech, 1960, 27: 740−743.

[10] DERUNTZ J A, HODGE P G. Crushing of a tube between rigid plates [J]. Trans ASME J App Mech, 1963, 30: 391−395.

[11] REID S R, REDDY T Y. Effect of strain hardening on the lateral compression of tubes between rigid plates [J]. Int J Solids Stru, 1978, 14: 213−225.

[12] GOTOH M, SHIBADA Y. Elasto-plastic finite element analysis for one and two dimensions of lateral compression of tube [C]// Spring Proceeding Plastic Working. Tokyo: Cho-Fu, 1989: 571−574.

[13] LEU D K. The shaping of a circular tube into a symmetric square-tube by finite-element modeling [J]. J Mat Proc Tech, 2006, 178: 287−296.

[14] YAMADA Y, YOSHIMURA N, SAKURAI T. Plastic stress-strain matrix and its application for the solution of elastic-plastic problems by the finite-element method [J]. Int J Mech Sci, 1968, 10: 343−354.

[15] MCMEEKING R M, RICE J R. Finite element formulations for problems of large elastic-plastic deformation [J]. Int J Solids Stru, 1975, 11: 601−606.

[16] YAMADA Y. Plasticity and visco-elasticity [M]. Japan: Baifukan, 1980.

[17] ODEN J T, PRIES E B. Nonlocal and nonlinear friction law and variational principles for contact problems in elasticity [J]. Trans ASME J Applied Mech, 1983, 50: 67−76.

(Edited by LI Xiang-qun)